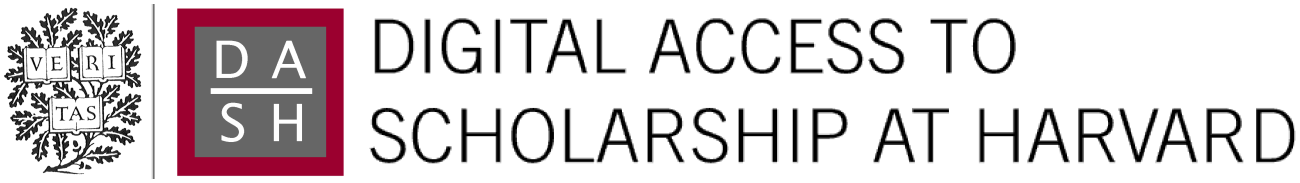

Kinked p–n Junction Nanowire Probes for High Spatial Resolution Sensing and Intracellular Recording

Kinked p-n Junction Nanowire Probes for High Spatial Resolution Sensing and Intracellular Recording

Zhe Jiang[1,†], *Quan Qing*[1,†], *Ping Xie*[†], *Ruixuan Gao*[†], *Charles M. Lieber**[†,‡]

[†]Department of Chemistry and Chemical Biology, Harvard University, Cambridge, Massachusetts 02138

[‡]School of Engineering and Applied Science, Harvard University, Cambridge, Massachusetts 02138

[1]These authors contributed equally to this work

*Corresponding authors: Email: cml@cmliris.harvard.edu

Abstract. Semiconductor nanowires and other semiconducting nanoscale materials configured as field-effect transistors have been studied extensively as biological/chemical (bio/chem.) sensors. These nanomaterials have demonstrated high-sensitivity from one- and two-dimensional sensors, although the realization of the ultimate point-like detector has not been achieved. In this regard, nanoscale p-n diodes are attractive since the device element is naturally localized near the junction, and while nanowire p-n diodes have been widely studied as photovoltaic devices, their applications as bio/chem. sensors have not been explored. Here we demonstrate that p-n diode devices can serve as a new and powerful family of highly localized biosensor probes. Designed nanoscale axial p-n junctions were synthetically introduced at the joints of kinked silicon nanowires. Scanning electron microscopy images showed that the kinked nanowire structures were achieved, and electrical transport measurements exhibited rectifying behavior with well-defined turn-on in forward bias as expected for a p-n diode. In addition, scanning gate microscopy demonstrated that the most sensitive region of these nanowires was localized

near the kinked region at the p-n junction. High spatial resolution sensing using these p-n diode probes was carried out in aqueous solution using fluorescent charged polystyrene nanobeads. Multiplexed electrical measurements show well-defined single-nanoparticle detection, and experiments with simultaneous confocal imaging correlate directly the motion of the nanobeads with the electrical signals recorded from the p-n devices. In addition, kinked p-n junction nanowires configured as three-dimensional probes demonstrate the capability of intracellular recording of action potentials from electrogenic cells. These p-n junction kinked nanowire devices, which represent a new way of constructing nanoscale probes with highly-localized sensing regions, provide substantial opportunity in areas ranging from bio/chem. sensing and nanoscale photon detection to three-dimensional recording from within living cells and tissue.

The rational design and synthesis of nanomaterials have enabled many advances in functional nanoelectronics,[1-9] and moreover, have opened-up unique opportunities at the interface between nanoelectronics and biological systems.[2,10-21] For example, recent studies have shown that nanoscale field-effect transistors (nanoFETs) can be synthetically encoded at the tips of kinked silicon nanowires.[2,5] These kinked nanostructures can be readily configured as three-dimensional (3D) bioprobes, which enabled recording intracellular action potentials from beating cardiomyocytes in a minimally-invasive manner.[2] This work represented the first demonstration of internalizing an active electronic probe, a transistor, which was comparable in size to viruses and many biological macromolecules inside a cell. While these studies open up a new paradigm for integrating electronics with cells and tissue, they are also potentially limited in that synthetic preparation of an ideal point-like nanoFET detector is challenging.

In this regard, nanoscale p-n diodes are attractive since the device element is naturally localized at the depletion region of the junction.[22] A number of previous studies have shown that p-n junctions can be synthetically encoded in axial and core/shell nanowires,[3-4,23-24] although only the photovoltaic

properties of such nanojunctions have been thoroughly studied.[3,4] Such p-n diodes have not yet been investigated as bio/chem. sensors. Here we report a successful synthetic integration of p-n junction in the kinked silicon nanowire structure, and study for the first time both experimentally and theoretically these devices as highly-localized electronic biosensors. In particular, we focus on the use of p-n junction kinked nanowire devices for charge sensing down to the single nanoparticle level, and for intracellular potential recording within live cells.

Kinked p-n junction silicon nanowires (SiNWs) were synthesized by gold nanoparticle-catalyzed chemical-vapor-deposition (CVD) process with doping and geometric control adapted from our previous report.[5, 25] Initially, boron-doped p-type SiNWs were grown for 15 minutes at a calibrated growth rate of 0.7 μm/min. The reactor was evacuated for ca. 15 s, and then growth was continued using phosphine dopant to create an n-type nanowire segment (forming the p-n junction) for 30 s, followed by a second cycle of reactor evacuation and continued growth using phosphine for ca. 15 min. Scanning electron microscopy (SEM) images of the SiNWs prepared in this way (Figure 1a) showed that the majority (> 90%) of the kinked nanowires have a 120° angle between the two arms, which is consistent with our previous results that the abrupt evacuation/resumption of feeding gases during the growth of n-type SiNWs introduces a 120° kink in high-yield.[5] In addition, analysis of images showed that a small fraction (< 10%) of the kinked nanowires exhibited a 60° angle (Figure S1), indicating that the switching between p- and n-dopant could also introduce a similar kink (with both in *cis* orientation[2]) albeit at a much lower yield. Here we focus on the 120° kinked SiNWs.

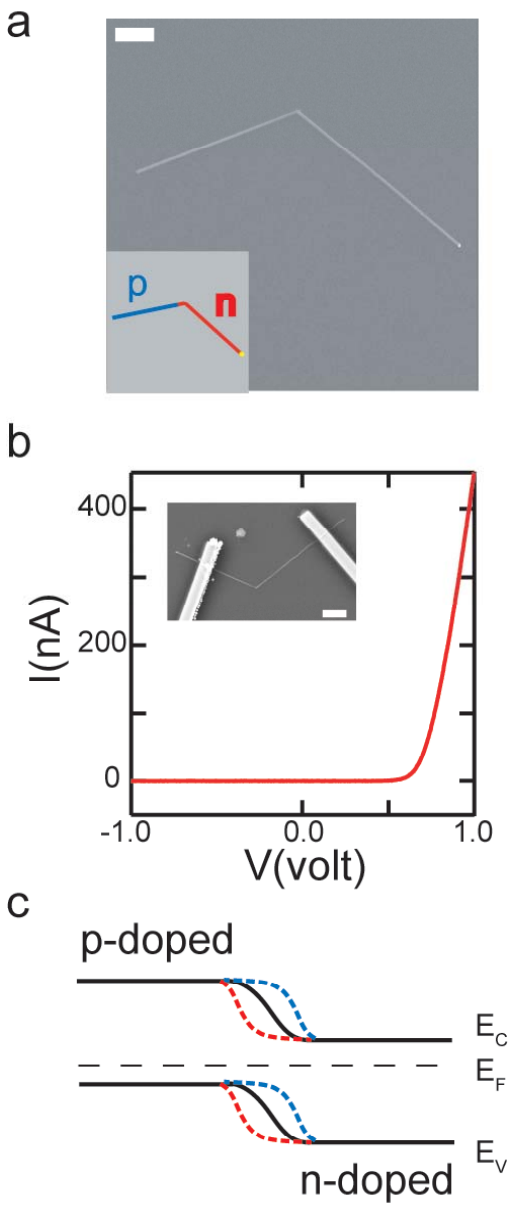

Figure 1. Design and controlled synthesis of kinked p-n nanowires. a, Representative SEM image of a kinked p-n SiNW with 120° tip angle. Scale bar, 1 □m. Inset: Schematic of a kinked p-n nanowire with 120° tip angle. The blue and red lines designate the p-doped and n-doped arms, respectively. **b,** Current vs. voltage (*I*-*V*) data recorded from a representative kinked p-n nanowire device. Inset: SEM image of the device structure. Scale bar, 2 □m. **c,** Schematic band diagram (black curves) and band diagram change of kinked p-n nanowires under gate potential. The blue and red dashed lines designate band diagram under negative and positive gate potentials respectively. E_C, E_V and E_F mark the position of the conduction band, valence band and Fermi energy, respectively.

To assess the overall electrical characteristics of the kinked p-n nanowires, contacts (Cr/Pd/Cr 1.5/120/60 nm) were defined on both arms by electron-beam lithography (EBL) and metallization[2,26] (inset, Figure 1b). Typical current versus voltage (I-V) data (Figure 1b) show clear rectification with no measurable current in reverse bias and an onset for current flow of 0.6 V in forward bias. These results are consistent with previously studies of straight SiNWs with axial p-n junctions.[4] In addition, measurements made on devices with two contacts per arm (Figure S2) showed that no metal/SiNW Schottky barriers were present and allowed the estimation of the dopant concentrations. Specifically, the dopant concentrations of the p-arm and n-arm were estimated to be ca. 9×10^{18} cm^{-3} and 9×10^{19} cm^{-3}, respectively. [26]

In a planar p-n diode device, the p-n junction is mostly buried beneath the surface and thus can only be partially gated with a top gate electrode.[28] In contrast, the axial design of our kinked nanowires fully exposes the nanoscale p-n junction to external potential and enables a much more effective gate modulation of the transport behavior. Figure 1c illustrates a schematic band diagram change of the nanowire diode when a gate potential is applied at the p-n junction. The heavily doped p- and n- arms are not affected by the gate and the Fermi energy is pinned along the nanowire. When a negative potential is applied, the electron energy levels in both the conduction band and the valence band are raised (Blue dashed lines in Figure 1c). As a result, the p-depletion region becomes more conductive, while the n-depletion region less conductive. In the case of applying a positive potential, the opposite occurs. In order to estimate the overall gate response of our device, we assume that (1) the carrier concentration distribution in the depletion region is linear, (2) the depletion region can be approximated as a number of small segments, each of which can be treated as a field-effect transistor with uniform doping, (3) the gate coupling is ideal, and (4) the width of the depletion region is the same as the abrupt junction. In addition, the mobility along the nanowire is treated as uniform, to simplify the calculation without affecting the physics. It follows that the resistance change (ΔR) of the p-n junction can be expressed as $\Delta R \propto \Delta V[\ln(N_A)/N_A^2 - \ln(N_D)/N_D^2]$ (see Supplementary Information), where ΔV is the change of the gate potential, and N_A and N_D are the dopant concentration of the p- and n-arms,

respectively. When N_A and N_D are equal or comparable, the p-n junction will behave as an ambipolar FET. However, when $N_A<N_D$, the p-n junction will function as a p-type FET, and similarly, when $N_A>N_D$, an n-type. In our design the doping level of the p-arm is ten times lower than the n-arm, thus the device is predicted to behave as a p-type FET.

Tip-modulated scanning gate microscopy (tmSGM)[29] was used to identify directly the gate response and length-scale of the sensitive regions in kinked p-n nanowire devices. Briefly, a conductive atomic force microscopy (AFM) tip was used as a local gate to modulate the conductance of the kinked p-n nanowire junction.[30] The conductance change was phase-locked to the vibration of the tip to enhance the spatial resolution,[29] and the conductance map at different tip biases was superimposed over the topological image of the device. Representative data (Figure 2a) show several key features. First, only the region close to the kink where the p-n junction was synthetically defined showed clear gate response. Second, the p-depletion region gave 3-5 fold larger conductance change than the n-depletion region (inset traces, Figure 2a). This result is consistent with our theoretical estimate using the calculated dopant concentration of the arms, and implies that the device behavior is similar to a p-type FET. Third, the length of the p-depletion region, which defines the spatial resolution of the device, was estimated from the full width at half maximum (FWHM) of the conductance line profiles along the nanowire axis (inset traces, Figure 2a) and found to be 210 nm.[30] While the size of the sensitive region without optimization is comparable to the best value reported in our previous work, we note that theoretical spatial resolution of a gated p-n device, characterized by the thickness of the depletion region, is 10-30 nm for highly doped silicon,[31] and thus could be improved in the future.

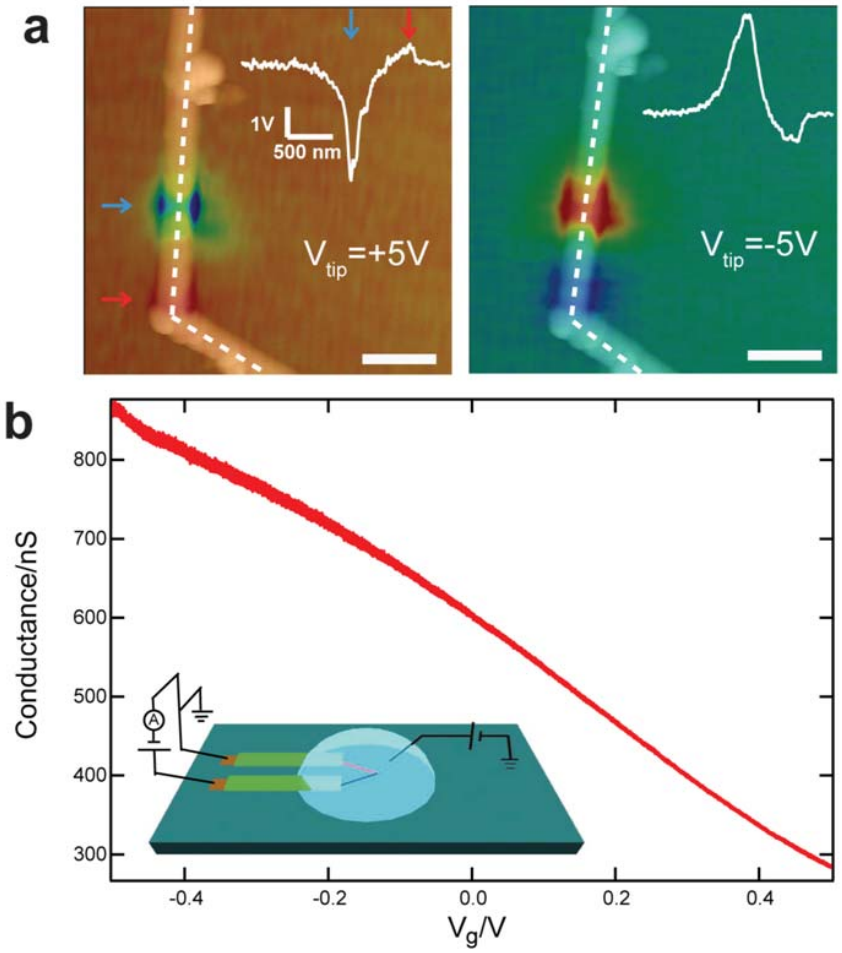

Figure 2. tmSGM and water-gate experiments of kinked p-n nanowire devices. a, Superposition of tmSGM images on AFM topographic images of a representative kinked p-n nanowire device under V_{tip} of +5 V (left, scanning direction from top down) and -5 V (right, scanning direction from bottom up), respectively. Scale bar, 0.5□m. The blue/red arrows indicate the p-type and n-type depletion/accumulation regions (left panel), respectively; the same positions show accumulation/depletion in the right panel. Insets: Line profiles of the tmSGM signal along the white dashed lines about these p-type and n-type regions. **b,** Conductance versus water-gate reference potential data recorded from a representative kinked p-n nanowire device in 1× phosphate buffer saline (PBS). Inset: Schematic of conductance vs. water-gate experiment.

The devices used for sensing experiments in solution were fabricated through multiple EBL, metallization and passivation steps similar to previous reports,[2,10,12,26] using Cr/Pd/Cr for contacts and SU8 as the passivation layer to isolate the metal electrodes from the aqueous medium. The sensitivity of kinked nanowire p-n devices in solution was assessed by water-gate experiments[2,10] (inset, Figure 2b),

where the p-n junction was forward biased at 1.0 V and a Ag/AgCl electrode was used to control the chemical potential (V_g) of the solution. Representative conductance versus V_g data (Figure 2b) demonstrate a p-type response and sensitivity of 620 nS/V. The p-type response is consistent with the tmSGM results. The water-gate results also exhibit an increase in noise with increasing device conductance, which could be due to increased recombination at higher carrier concentrations within the depletion region.[22] From a practical perspective, such water-gate data can be used to choose an optimal operating regime (i.e., where the sensitivity:noise ratio is maximized), although future work should also address fundamental origin of noise in these p-n junction nanowire devices and potential reductions through, for example, improvements in junction quality and reduction of the surface defects.

Localized detection using our kinked p-n probes was first explored in single nanoparticle sensing experiments. Specifically, an array of kinked p-n nanowires probes on a SiO_2 substrate [2,10,12] was coupled to poly(dimethylsiloxane) (PDMS) microfluidic channel to control the solution flow over the devices.[32] Conductance versus time traces recorded simultaneously from two independent devices following the introduction of a 1.2 nM solution of 100 nm diameter charged fluorescent polystyrene nanobeads (Figure 3a) exhibit several key features. First, when nanobeads solutions flow through the device area, uncorrelated 'pulse' (on/off) signals were observed from both devices (red traces, Figure 3a). The time duration time of the 'on' state of the pulses ranged from 50 to 200 ms. Second, the conductance amplitudes of signals recorded on device-1 (D1) and device-2 (D2) were consistently 3-4 and 2-3 nS, respectively. The calibrated potential change (based on the water-gate sensitivity of the two devices) yields a consistent decrease of 5-6 mV at the p-n junction of both devices. This decrease in potential is also consistent with the negative charge on the nanobeads.[33] Third, introduction of the aqueous solution without nanobeads (green traces, Figure 3a) exhibited no on/off pulsed signals from either device even over much longer recording times. Together, these results are consistent with the detection of single nanobeads as outlined schematically in Figure 3b. Briefly, when there is no nanobead close to the p-n junction within the Debye screening length, the conductance of the device remains constant (left image, Figure 3b). When a nanobead approaches and/or attaches to the p-n

junction, an increase of conductance will be observed due to the negative charges on the nanobead[33] (middle image, Figure 3b), and when the nanobead leaves the sensitive region of the probe, the conductance returns to baseline (right image, Figure 3b).

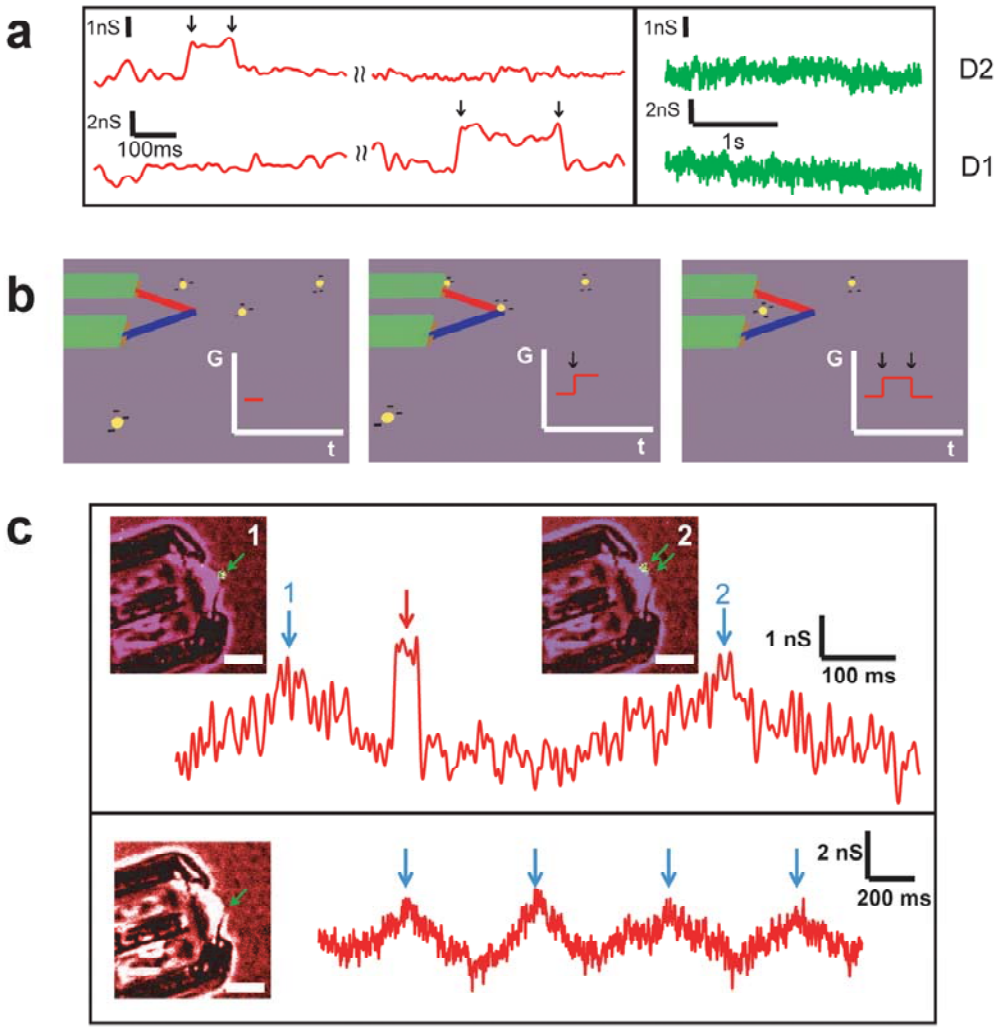

Figure 3. Fluorescent polystyrene nanobead sensing experiment. a, (Left) Conductance vs. time data recorded simultaneously from two independent kinked p-n nanowire devices with nanobeads in deionized (DI) water introduced into the microfluidic channel. Black arrows mark the on/off points of the signals. (Right) Conductance vs. time data recorded simultaneously from the same two devices with only DI water in the microfluidic channel. **b**, Schematic of fluorescent polystyrene nanobead sensing process using kinked p-n nanowire devices and the corresponding schematic of time-dependent change in device conductance. Black arrows mark the on/off points of the signal. **c**, (Top) Simultaneous confocal microscopy and conductance vs. time data recorded from a kinked p-n nanowire device in a nanobead solution flow. Red arrow marks the charge sensing signal. Blue arrows mark

the photocurrent peaks caused by the laser scanning over the p-n junction for images 1 and 2. The green arrows in the images highlight the positions of the nanowire junction and fluorescent nanobead in both images. In Image 1, the two green arrows overlap. (Bottom) Simultaneous confocal microscopy and conductance vs. time data recorded from the same device without nanobeads in solution. Blue arrows indicate photocurrent peaks due to the laser scanning over the p-n junction. The green arrow in the image highlights the position of the nanowire junction. All the electrical data were filtered through a 100Hz low-pass digital filter. Scale bars, 5□m.

To confirm this interpretation of the multiplexed electrical measurements we carried out simultaneous confocal fluorescent microscopy imaging and electrical recording in the presence and absence of the fluorescent nanobeads.[32] Significantly, we find that a conductance pulse (red arrow, Figure 3c) similar to that observed in measurements described above occurs when a single nanobead approaches the p-n junction at the elbow of the kink (inset-1) and then diffuses away (inset-2). The 50 ms wide conductance pulse is consistent with brief contact between the nanobead and the p-n junction during this process. We also note that when the laser scans over the p-n junction, there is a photocurrent (conductance increase) as indicated by blue arrows 1 and 2 (Figure 3c), and this can be used to assign the times when each image is captured. In addition, when the same solution without fluorescent nanobeads was introduced into the device, only periodic photocurrent was observed (lower trace, Figure 3c). These control experiments further confirm that conductance pulses correspond to single nanobead detection, and also highlight the potential of our p-n devices as point-like nanoscale photodetectors for biophysical studies and imaging.

We have also configured the kinked p-n junction nanowires as three-dimensional (3D) probes for highly localized interaction with living cells (Figure 4a). The 3D p-n junction devices were fabricated using procedures similar to our previous studies[2] to yield nanowire probe oriented at 45-60^{o} angle with respect to the substrate. In a typical experiment, the 3D p-n junction nanowire probes were functionalized with 1,2-dimyristoyl-sn-glycero-3-phosphocholine (DMPC) bilayer and then embryonic chicken cardiomyocyte cells cultured on a PDMS sheet were positioned over a nanowire probe within a cell perfusion chamber.[2,34] Representative conductance versus time data recorded from a spontaneously

beating cardiomyocyte cell (Figure 4b; Figure S3) initially show an approximately 20 mV shift as the probe transitions from the extracellular region to the intracellular rest potential, which is consistent with our previous studies,[2] followed by the development of periodic spikes with the same frequency of the overall cell contraction, and an amplitude, shape and time scale of individual peaks characteristic of the intracellular action potential. Specifically, a reproducible fast onset of over 60 mV increase in local potential is observed followed by a broad slow return to baseline within 200 ms, which are consistent with the intracellular action potentials recorded using a patch clamp.[35] These results show that the nanoscale p-n diode sensor can be internalized by the cell. In addition, we find that these nanowire p-n junction probes can be inserted and retracted multiple times from the same cell without losing key features of the intracellular action potential or loss of cell viability, highlighting the minimal invasiveness of these nanoscale probes. We note that the highly localized nature of our p-n kinked probe could enable detailed studies of the potential distribution within the cell and in subcellular structures. However, the current probe design does not provide sufficient control of the probe-cell position for such experiments due to the flexibility of the floating PDMS cell substrate.

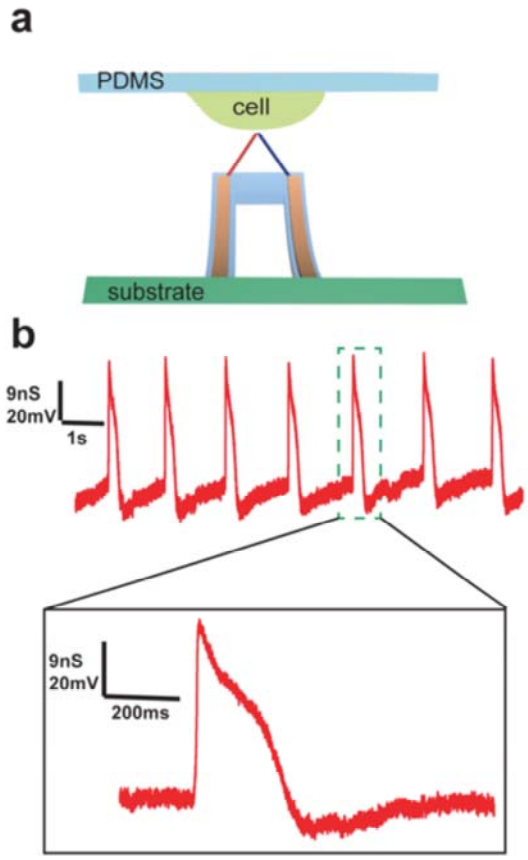

Figure 4. Intracellular electrical recording from spontaneously beating chicken cardiomyocytes. a, Schematic of intracellular recording from spontaneously beating embryonic chicken cardiomyosytes cultured on PDMS substrate using 3D kinked p-n nanoprobes. **b**, (Top) Steady-state intracellular recording using a 3D kinked p-n nanoprobes from a spontaneously beating cardiomyocyte cell. (Bottom) Zoom of the single action potential peak from the green-dashed region.

In conclusion, we have demonstrated for the first time that a nanoscale axial p-n junction synthetically embedded in a kinked nanowire structure can be tuned to work as a highly localized field-effect sensor to detect charges down to a single nanoparticle level, and to record full intracellular signals of spontaneously beating cardiomyocyte cells. Compared to previously reported nanoFET probes,[2] this gateable p-n diode device represents a new family of nanoscale biosensor probes with several unique advantages, including (1) a highly localized sensing region that can be tuned simply by optimizing the doping levels of the p- and n-arms, (2) the possibility of yielding different types of field-effect sensors (i.e., p-type, n-type and ambi-polar) by tuning the relative doping ratio between the p- and

n-arms, and (3) the potential of using the p-n junction as a 3D nanoscale photodetector, for example, to study highly localized fluorescent events when integrated within living cells and tissue.

Acknowledgements. C.M.L. acknowledges support of this research from a NIH Director's Pioneer Award (1DP1OD003900).

References & Notes.

1. Timko, B. P.; Cohen-Karni, T.; Qing, Q.; Tian, B.; Lieber, C. M. *IEEE Trans. Nanotechnol.* **2009**, DOI: 10.1109/TNANO.2009.2031807
2. Tian, B.; Cohen-Karni, T.; Qing, Q.; Duan, X.; Xie, P.; Lieber, C. M. *Science* **2010**, *329*, 830-834.
3. Tian, B.; Zheng, X.; Kempa, T. J.; Fang, Y.; Yu, N.; Yu, G.; Huang, J.; Lieber, C. M. *Nature* **2007**, *449*, 885-890.
4. Kempa, T. J.; Tian, B.; Kim, D. R.; Hu, J.; Zheng, X.; Lieber, C. M. *Nano Lett.* **2008**, *8*, 3456-3460.
5. Tian, B.; Xie, P.; Kempa, T. J.; Bell, D. C.; Lieber, C. M. *Nature Nanotech.* **2009**, *4*, 824-829.
6. Xu, S.; Qin, Y.; Xu, C.; Wei, Y.; Yang, R.; Wang, Z. L.; *Nature Nanotech.* **2010**, *5*, 366-373.
7. Yan, H.; Choe, H. S.; Nam, S. W.; Hu, Y.; Das, S.; Klemic, J. F.; Ellenbogen, J. C.; Lieber, C. M. *Nature* **2011**, *470*, 240-244.
8. Dick, K. A.; Deppert, K.; Larsson, M. W.; Martensson, T.; Seifert, W.; Wallenberg, L. R.; Samuelson, L. *Nat. Mater.* **2004**, *3*, 380-384.
9. Jiang, X.; Tian, B.; Xiang, J.; Qian, F.; Zheng, G.; Wang, H.; Mai, L.; Lieber, C. M. *Proc. Natl. Acad. Sci. U.S.A.* **2011**, *108*, 12212-12216.
10. Qing, Q.; Pal, S. K.; Tian, B.; Duan, X.; Timko, B. P.; Cohen-Karni, T.; Murthy, V.N.; Lieber, C. M. *Proc. Natl. Acad. Sci. USA*, **2010**, *107*, 1882-1887.

11. Cohen-Karni, T.; Timbo, B. P.; Weiss, L. E.; Lieber, C. M. *Proc. Natl. Acad. Sci. USA*, **2009**, *106*, 7309-7313.

12. Cohen-Karni, T.; Qing, Q.; Li, Q.; Fang, Y.; Lieber, C. M. *Nano Lett.* **2010**, *10*, 1098-1102.

13. Heller, I.; Smaal, W. T. T.; Lemay, S. G.; Dekker, C. *Small* **2009**, *5*, 2528-2532.

14. Kotov, N. A.; Winter, J. O.; Clements, I. P.; Jan, E.; Timko, B. P.; Campidelli, S.; Pathak, S.; Mazzatenta, A.; Lieber, C. M.; Prato, M.; Bellamkonda, R. V.; Silva, G. A.; Kam, N. W. S.; Patolsky, F.; Ballerini, L. *Adv. Mater.* **2009**, *21*, 3970-4004.

15. Patolsky, F.; Timko, B. P.; Yu, G.; Fang, Y.; Greytak, A. B.; Zheng, G.; Lieber, C. M. *Science* **2006**, *313*, 1100-1104.

16. Lieber, C. M. *MRS Bull*. **2011**, *36*, 1052-1063.

17. Patolsky, F.; Timko, B. P.; Zheng, G. F.; Lieber, C. M. *MRS Bull*. **2007**, *32*, 142-149.

18. Timko, B. P.; Cohen-Karni, T.; Yu, G.; Qing, Q.; Tian, B.; Lieber, C. M. *Nano Lett*. **2009**, *9*, 914-918.

19. Pui, T. S.; Agarwal, A.; Ye, F.; Balasubramanian, N.; Chen, P. *Small* **2009**, *5*, 208-212.

20. Eschermann, J. F.; Stockmann, R.; Hueske, M.; Vu, X. T.; Ingebrandt, S.; Offenhäusser, A. *Appl. Phys. Lett.* **2009**, *95*, 083703-1-083703-3.

21. Stern, E.; Klemic, J. F.; Routenberg, D. A.; Wyrembak, P. N.; Turner-Evans, D. B.; Hamilton, A. D.; LaVan, D. A.; Fahmy, T. M.; Reed, M. A. *Nature* **2007**, *445*, 519-522.

22. Sze, S. M. *Semiconductor devices, physics and technology*; Wiley: Singapore, 2002, pp 84-130.

23. Gudlksen, M. S.; Lauhon, L. J.; Wang, J.; Smith, D. C.; Lieber, C. M. *Nature* **2002**, *415*, 617-620.

24. Lauhon, L. J.; Gudlksen, M. S.; Wang, D.; Lieber, C. M. *Nature* **2002**, *420*, 57-61.

25. Kinked p-n silicon nanowires were synthesized by chemical-vapor deposition (CVD) through a nanoparticle-catalyzed vapor-liquid-solid (VLS) process as described previously.[5] Specifically, 100 nm diameter gold nanoparticles (Ted Pella) were dispersed on Si growth substrates with 600

nm SiO_2 layer (Nova Electronic Materials). Growth of heavily boron-doped p-type arm was first carried out by feeding SiH_4 (1 sccm), B_2H_6 (10 sccm, 100 ppm in H_2) and H_2 (60 sccm) into the system for 15 minutes at a total pressure of 40 torr and temperature of 450°C. The growth was then paused for 15 seconds, by rapidly evacuating the chamber to lowest pressure and shutting off the gas lines. SiH_4 (1 sccm), PH_3 (4 sccm) and H_2 (60 sccm) were then flown into the system at the same total pressure and temperature to grow a heavily doped n-type section for 30 seconds, forming the p-n junction. A second evaculation of 15 seconds followed, and finally the heavily doped n-type arm was allowed to finish in additional 15 minutes.

26. Two pairs of metal electrodes (1.5 nm Cr/120 nm Pd/60 nm Cr, spacing between electrodes 1.5 μm) were fabricated on each of the p- and n-type arms of a kinked nanowire device. The diameter of the nanowire was 100 nm. The doping levels of the arms were estimated using $N=\sigma/q\mu$, where N is the doping level, σ is the conductivity calculated from the slope of the I_{ds}-V_{ds} trace in Figure S2, q is the charge of an electron, and μ is the mobility. Here we take μ as 14 $cm^2/V\bullet s$ [27].

27. Cui, Y.; Zhong, Z.; Wang, D.; Wang, W. U.; Lieber, C. M.; *Nano Lett.* **2003**, *3*, 149-152.

28. Rusu, A.; Bulucea, C. *Proc. Rom. Acad.* **2009**, *10*, 285-290.

29. Wilson, N. R.; Cobden, D. H. *Nano Lett.* **2008**, *8*, 2161-2165.

30. The device chip was mounted on a BioScope MultiMode SPM stage (Digital Instrument). A constant current of 250-700 nA was injected into the kinked p-n device, resulting in a forward bias of ~1V. The voltage drop across the device was measured using a low-noise differential preamplifier (SR560, Stanford Research Systems). A conductive AFM tip (ARROW-CONTPT-10, NanoWorld) vibrating at a resonance frequency of 90 kHz was used as a local gate and scanned over the device to map the conductance image in "Lift Mode". Specifically, first, for each scan line, zero potential was applied to the tip, and a topographic image was acquired in Tapping Mode with feedback enabled. The tip was then lifted up 30 nm, and a tip potential of +/- 5 V was applied. The tip was scanned across the same line again following the captured

topological profile with feedback turned off, when the change of voltage across the device was recorded with a lock-in amplifier (SR830, Stanford Research Systems) using the tip oscillation as the reference frequency.[29] In order to remove the drift error during the imaging, we scanned in opposite directions for V_{tip}=+5V (FWHM=120 nm) and V_{tip}=-5V (FWHM=300 nm) images, and obtain the average of 210 nm as the corrected length of the sensitive region for our device.

31. Weber, L.; Gmelin, E. *Appl. Phys. A* **1991**, *53*, 136–140.

32. To control the solution flowing over the devices, a 1.7 mm thick polydimethylsiloxane (PDMS) sheet with a micro-fluidic channel 50 μm in height and 1 mm in width was put on the device chip. Fluorescent polystyrene nanobeads of 100 nm in diameter (initial concentration 24nM in DI water, excitation wavelength 540nm, emission wavelength 560nm, from Phosphorex) were diluted in DI water (1:20), and introduced into the micro-fluidic channel at a flow rate of 0.02 ml/hour set by a syringe pump (PHD 2000, Harvard Apparatus). A confocal fluorescent microscope (FV1000, Olympus) was used to image the motion of the fluorescent nanobeads and the kinked probes in real time while the conductance was recorded. Real-time fluorescent images of the p-n junction area were captured at a rate of 2 Hz using a 559 nm laser to excite the nanobeads. Two channels with filters of 490-540 nm and 575-675 nm were recorded together to rule out noise signals and unambiguously identify the nanobeads. Images were then superimposed over the device image recorded with a 535-565 nm filter to mark the relative position of the nanobeads and the p-n junction.

33. The Zeta potential of the nanobeads was measured using PALS Zeta Potential Analyzer (Brookhaven Instruments). An averaged zeta potential of -59±11 mV from 6 runs was obtained.

34. Embryonic chicken cardiomyocytes were cultured using published protocols on thin PDMS films[2,11]. Device chips were incubated with lipid vesicles of 1,2-dimyristoyl-sn-glycero-3-phosphocholine (DMPC, Avanti Polar Lipids Inc.) containing 1% 1-myristoyl-2-{12-[(7-nitro-2-1,3-benzoxadiazol-4-yl) amino] dodecanoyl}-sn-glycero-3-phosphocholine (NBD-lipid, Avanti Polar Lipids Inc.) as fluorescent reporter to form lipid bilayers over the nanowire surface, using

a procedure described earlier. [2] The cell recording measurements were carried out in Tyrode solution (Sigma Aldrich) at 35°C. The devices were forward biased at 1.0 V, and the current was converted to voltage with a current preamplifier (Model 1211, DL Instruments) at sensitivity of 10^{-6} A/V, before low-pass filtered (0-6KHz, CyberAmp 380, Molecular Devices), and digitized at 20 kHz sampling rate (Axon Digi1440A, Molecular Devices). A Ag/AgCl reference electrode was used to fix the extracellular solution potential at a constant value of +0.3V in all recording experiments[2,11]. The PDMS/cell sheets were manipulated using a glass micropipette mounted on a micromanipulator, to control the relative position between the cells and the nanowires as previously reported [2,11].

35. Zipes, D.P.; Jalife, J. *Cardiac Electrophysiology: From Cell to Bedside*; Saunders: Philadelphia, 2009.

TOC Graphic

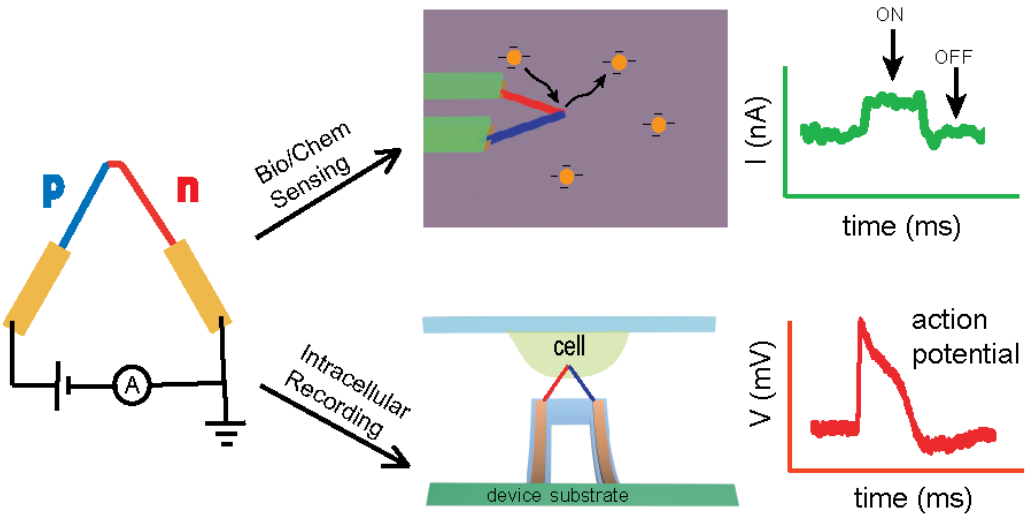
P
n
A
Bio/Chem
Sensing
Intracellular
Recording
cell
device substrate
ON
OFF
I (nA)
time (ms)
V (mV)
action
potential
time (ms)

Supplementary information for:

Kinked p-n Junction Nanowire Probes for High Spatial Resolution Sensing and Intracellular Recording

Zhe Jiang, Quan Qing, Ping Xie, Ruixuan Gao, Charles M. Lieber

This file includes:

Semi-quantitative model for device sensitivity

We first use n-type depletion region as an example of calculating resistance change of p-n junction under gating potential. We have: $\sigma_n = nq\mu$, $n = N_C e^{-(E_C - E_F)/kT}$, where σ is the electrical conductivity, n is the carrier concentration of electrons, q is the charge of an electron, μ is the mobility of electrons, N_c is the density of states at the conduction band edge. Assuming that carrier concentration distribution within the depletion region along the nanowire is linear ($n = n_i + lk_D$), it follows that:

$$\Delta\sigma_n = \Delta nq\mu = nq\mu(\Delta Vq/kT) = \Delta Vq\sigma_n/kT$$

$$\Delta\rho_n = -\Delta\sigma_n/\sigma_n^2$$

$$\Delta\rho_n = -\Delta V/(n\mu kT) = -\Delta V/[(n_i + lk_D)\mu kT]$$

$$\Delta R_n = \int_0^{l_D} \frac{\Delta\rho_n}{\pi r^2} dl = \int_0^{l_D} -\frac{\Delta V}{\pi r^2 \mu kT[(n_i + lk_D)]} dl = -\frac{\Delta V}{\pi r^2 \mu kTk_D} Ln(\frac{N_D}{n_i})$$

, where ρ and R are the resistivity and resistance, respectively.

Using the same method, we can have resistance change of the p-type depletion region as:

$$\Delta R_p = \int_{-l_A}^{0} \frac{\Delta\rho_p}{\pi r^2} dl = \int_{-l_A}^{0} \frac{\Delta V}{\pi r^2 \mu kT[(n_i - lk_A)]} dl = \frac{\Delta V}{\pi r^2 \mu kTk_A} Ln(\frac{N_A}{n_i})$$

So the total resistance change can be expressed as:

$$\Delta R = \Delta R_n + \Delta R_p = \frac{\Delta V}{\pi r^2 \mu kT}[\frac{1}{k_A} Ln(\frac{N_A}{n_i}) - \frac{1}{k_D} Ln(\frac{N_D}{n_i})]$$

, thus

$$\Delta R = \frac{\Delta V}{\pi r^2 \mu kT}[\frac{l_A}{N_A} Ln(\frac{N_A}{n_i}) - \frac{l_D}{N_D} Ln(\frac{N_D}{n_i})]$$

Because: $l_D N_D = l_A N_A$, $l_D k_D \cong N_D$, $l_A k_A \cong N_A$

We have: $\frac{k_D}{k_A} = (\frac{N_D}{N_A})^2$, and $\Delta R \cong A\Delta V[\frac{1}{N_A^2} Ln(N_A) - \frac{1}{N_D^2} Ln(N_D)]$

When $N_D > N_A$ and $\Delta V > 0$, $\Delta R > 0$, the device behaves as a p-type FET

When $N_D < N_A$ and $\Delta V > 0$, $\Delta R < 0$, the device behaves as an n-type FET

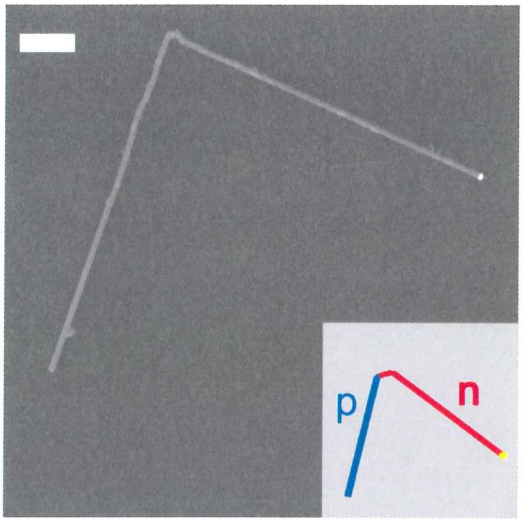

Figure S1. Representative SEM image of a kinked p-n SiNW with a 60° overall geometry (yield <10%). Scale bar, 1 μm. Inset: Schematic of the structure of kinked p-n nanowires with 60° tip angles. The blue and red lines designate the p-doped and n-doped arms, respectively. The 60° angle is the result of introducing two 120° kinks in a *cis* arrangement in the nanowire as described previously (see ref. 2, main text). Further studies to optimize the growth conditions will be needed to increase the yield of the 60° kinked nanowires.

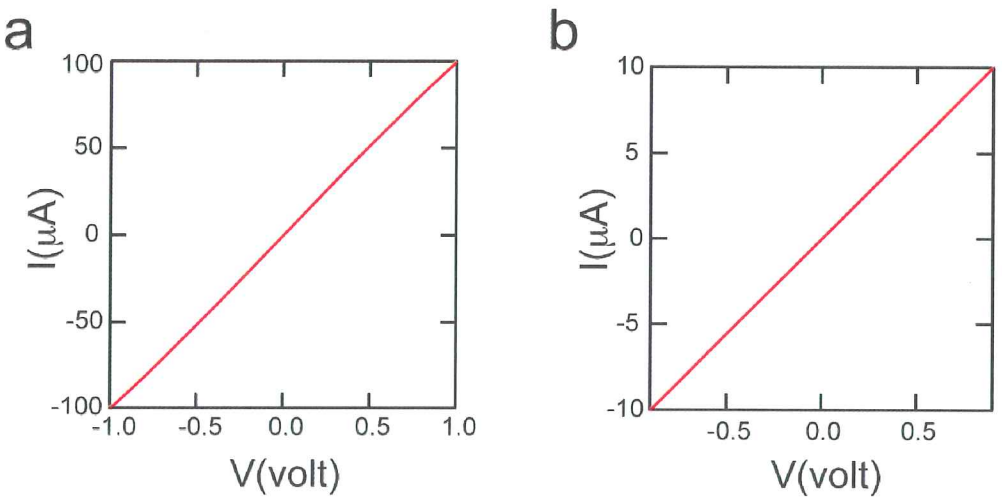

Figure S2. Arm conductance of kinked p-n nanowires. a, *I-V* data recorded from the n-type arm of a representative kinked p-n nanowire device. The spacing between electrodes was 1.5 μm. No barrier was present at metal contact. Dopant concentration of n-type arm was estimated to be 9×10^{19} cm^{-3}. **b**, *I-V* data recorded from the p-type arm of the same device. The spacing between electrodes was 1.5 μm. No barrier was present at metal contact. Dopant concentration of p-type arm was estimated to be 9×10^{18} cm^{-3}.

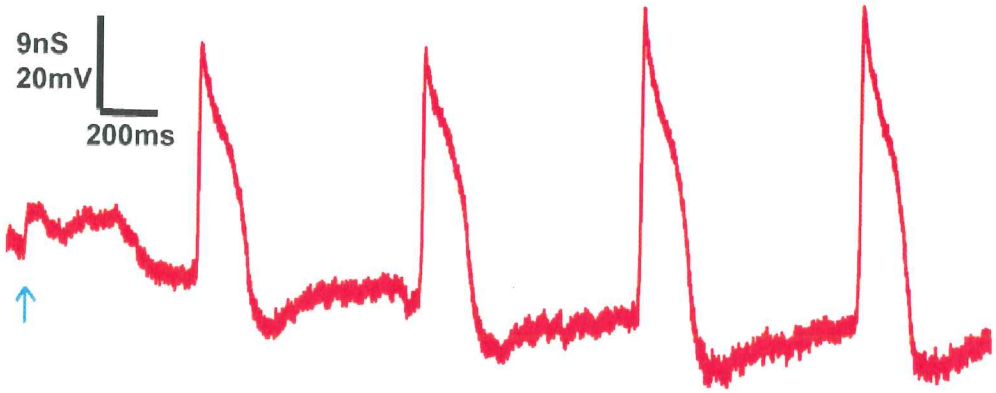

Figure S3. Transition from extracelluar to intracellular recording. The blue arrow marks the initial transition to intracellular signals. The calculated base line shift is ~20 mV.